# 博士論文

**Traction force and its regulation during cytokinesis in *Dictyostelium* cells**
（細胞性粘菌の細胞質分裂時のトラクションフォースとその制御機構）

2017年 9月

エムディ　ゴラム　サロワー　ジャハン
**Md. Golam Sarowar Jahan**

山口大学大学院医学系研究科

# Index



Abbreviations used in this paper:

GFP, green fluorescent protein; PTEN, phosphatase and tensin homolog

## Summary

Cytokinesis is the final stage of cell division. *Dictyostelium* cells have multiple modes of cytokinesis, including cytokinesis A, B and C. Cytokinesis A is a conventional mode, which depends on myosin II in the contractile ring. Myosin II null cells divide depending on substratum-attachment (cytokinesis B) or in a multi-polar fashion independent of the cell cycle (cytokinesis C). We investigated the traction stress exerted by dividing cells in the three different modes using traction force microscopy. Here, the traction stress is the unit force per unit area. In all cases, the traction forces were directed inward from both poles. Interestingly, the traction stress of cytokinesis A was the smallest of the three modes. Latrunculin B, an inhibitor of actin polymerization, completely diminished the traction stress of dividing cells, but blebbistatin, an inhibitor of myosin II ATPase, increased the traction stress. Myosin II is proposed to contribute to the detachment of cell body from the substratum. When the cell-substratum attachment was artificially strengthened by a poly-lysine coating, wild type cells increased their traction stress in contrast to myosin II null and other cytokinesis-deficient mutant cells, which suggests that wild type cells may increase their own power to conduct their cytokinesis. The cytokinesis-deficient mutants frequently divided unequally, whereas wild type cells divided equally. A traction stress imbalance between two daughter halves was correlated with cytokinesis failure. We discuss the regulation of cell shape changes during cell division through mechanosensing.

## Introduction

Cytokinesis is the final stage of cell division, which physically divides the cytoplasm of a parental cell into two daughter cells. The proper development and maintenance of the tissue architecture depend on successful cell division. Moreover, failure in cytokinesis results in abnormal polyploidy, which may promote tumorigenesis (Fujiwara et al., 2005).

The furrow ingression through the constriction of the actomyosin contractile ring has been recognized as the major mechanism of animal cell division (purse string model); however, there are other parallel mechanisms of division in social amoeba *Dictyostelium* cells and animal cells. Myosin II null cells of *Dictyostelium* cannot divide in suspension culture and become multinucleate because of their deficiency in the constriction of the cleavage furrow (De Lozanne and Spudich, 1987; Knecht and Loomis, 1987). However, they divide on the substratum depending on substratum attachment, which has been termed “attachment assisted mitotic cleavage” (Neujahr et al., 1997). Zang et al. (1997) referred to the cytokinesis in wild-type cells as “cytokinesis A” and the cytokinesis in myosin II null cells as “cytokinesis B”.

After shaking the culture, when large multinucleate HS1 cells are placed on a substratum, they adhere to the substratum and extend multiple leading edges. The activities of the leading edges tear the large cells into multiple fragments, with each fragment containing a nucleus. Spudich (1989) referred to this process as “traction mediated cytofission”. This cytofission occurs in a manner unrelated to the cell cycle; in many cases, the multinucleate cells divide via interphase cytofission. Uyeda et al. (2000) subsequently termed this process “cytokinesis C” to distinguish it from cytokinesis A and B. There is increasing evidence that higher animal cells also divide by cytokinesis B and C (Kanada et al., 2005; Choudhary et al., 2013). Figure 1 summarizes the three distinct modes of cytokinesis in *Dictyostelium* on substratum.

For cytokinesis B and C, cells are thought to exert a traction force against the substratum without actomyosin-dependent constriction of the contractile ring: two daughter cells are split by their migration toward opposite directions. However, there has been no direct observation of the traction force of these cells. Wild type cells may divide in both suspension and on substratum; however, on substratum, they appear to divide not only by constriction of the contractile ring but also through the use of traction forces (Nagasaki et al., 2002; Tanimoto and Sano, 2012).

Mechanosensing is a vital cellular process that enables cells to sense the physical properties of their surrounding microenvironments and adapt to mechanical changes in the microenvironments through mechanotransduction. Mechanosensing is an integral part of many processes, including hearing, blood-pressure regulation, muscle growth, bone remodeling, and cell shape control (Kee and Robinson, 2008). Mechanosensing and the mechanical feedback loop also regulate the cell shape during cytokinesis (Effler et al., 2006), and this loop requires a sensor and transducer. The potential mechanosensors include entire actin networks linked to the focal adhesion complex, stretch-activated membrane channels, and motor proteins (Martinac, 2004; Tamada et al., 2004; Effler et al., 2006; Orr et al., 2006). Myosin II has also been demonstrated to mediate cellular-scale mechanosensing during cell division (Effler et al., 2006; Pramanik et al., 2009; Ren et al., 2009). We have previously shown that PTEN (phosphatase and tensin homolog) is a mechanosensing signal transducer for myosin II localization in *Dictyostelium* cells (Pramanik et al., 2009). PTEN is a ubiquitous tumor suppressor protein, and its protein phosphatase activity regulates cell adhesion, cytokinesis, cell polarity of migration, spreading and growth (Funamoto et al., 2002; Iijima and Devreotes, 2002).

The traction force has been visualized and measured using various methods. The pioneering work visualized traction forces exerted by fibroblasts on very thin sheets of cross-linked silicone

fluid as elastic distortion and wrinkle of this substratum (Harris et al., 1980). In more recently improved methods, cells are placed on an elastic substratum, such as hydrogel, silicone gel or polyacrylamide gel, which are labeled with fluorescent makers, such as fluorescent beads. When cells exert a mechanical force, the substratum deforms, and the quantitative traction stress (force per unit area) is calculated from the displacement of the fluorescent markers (Lee et al., 1994; Oliver et al., 1994; Uchida et al., 2003; Iwadate and Yumura, 2008). These methods have been established as 'traction force microscopy', which enables reproducible and accurate traction stress measurements with high resolution.

In the present study, we investigated the traction stresses of the three modes of cytokinesis in *Dictyostelium* cells using traction force microscopy. The traction stresses were directed inward from both polar regions. Interestingly, the stresses of cytokinesis A were the smallest of the three modes. Myosin II null cells exerted a higher traction stress than the wild type cells. To understand the underlying molecular mechanism of this apparent contradiction, the cell substratum attachment was artificially increased by coating the substratum with poly-lysine. The wild type cells increased their traction stress in contrast to the myosin II null cells, which suggests that wild type cells may increase their own power to conduct their cytokinesis. PTEN null cells and other cytokinesis-deficient mutants also did not increase the traction stress with the increase of substratum adhesiveness. These mutants frequently divided unequally, whereas wild type cells divided equally. An imbalance of the traction force between two daughter halves was identified during the failure of cytokinesis. We will discuss the regulation of cell shape changes during cell division through mechanosensing.

## Materials and Methods

### Cell culture

*Dictyostelium discoideum* wild type (AX2) cells, myosin II null (HS1) cells, PTEN null cells, HS1 cells that expressed 3ALA myosin II, cortexillin A/B null cells, and Rac E null cells were cultured at 22°C in plastic dishes that contained HL5 medium (1.3% bacteriological peptone, 0.75% yeast extract, 85.5 mM D-glucose, 3.5 mM $Na_2HPO_4$, and 3.5 mM $KH_2PO_4$, pH 6.3). Extrachromosomal vector to express GFP-lifeact was transformed in the cells via electroporation, as previously described (Yumura et al., 1995). The GFP-lifeact plasmid was constructed by T. Q. P. Uyeda. Transformed cells were selected in HL5 medium that contained 10 μg/ml blasticidin S hydrochloride (Wako) in plastic dishes.

### Cell fixation and staining

Cells were fixed and stained with anti-myosin II antibody, tetramethyl rhodamine isothiocyanate (TRITC)-phalloidin and 4', 6-diamidino-2-phenylindole (DAPI), as previously described (Itoh and Yumura, 2007; Yumura et al., 1984).

### Fabrication of elastic substrata

Clear and colorless elastic substratum was prepared from a pair of liquid silicones, CY52-276A and CY52-276B (Dow Corning Toray), via modification of a previously described method (Iwadate and Yumura, 2008). A 300-mg aliquot of CY52-276A and a 250-mg aliquot of CY52-276B were thoroughly mixed. A small volume (3 μl) of the mixture was placed on a coverslip (No. 1; Matsunami) and evenly spread using a spinning rotor. The thickness of the silicone layer was approximately 15 μm. The silicone substratum on the coverslip was allowed to solidify at room temperature (22°C) for 14 hrs and was subsequently incubated at 70°C for 30 min. The

substratum was further maintained in a sealed container with a 400-µl aliquot of 3-aminopropyl triethoxysilane (Sigma-Aldrich) to attach the silane to the surface of the silicone substrata via vapor deposition. A plastic chamber with a hole (16 mm in diameter and 2 mm in depth) and silicone sheet (1 mm in thick) with a hole (16 mm in diameter) were assembled with the coverslip. A 200-µl aliquot of a solution that contained carboxylated red fluorescent microspheres (40 nm in diameter, F-8793, Molecular Probes) diluted 16,000 times with distilled water was added to the surface of silicone substratum. After approximately 3 min, the unattached beads were washed off with distilled water. The Young's modulus of the elastic substrata (1 kPa) was measured as previously described (Iwadate and Yumura, 2008).

**Microscopy**

Cells that expressed GFP-lifeact were plated on a silicone substratum with fluorescent red beads and observed using a DeltaVision microscope system (GE Healthcare Life Sciences) based on an inverted microscope (IX71, Olympus) with an objective lens (PlanApo N 60x, NA 1.42, Olympus). Movies were obtained in 30 sec intervals in green fluorescence (for GFP), red fluorescence (for beads) and differential interference contrast (DIC) channels as z-stacks at 1-µm intervals. The exposure times for GFP, beads and DIC were set as 0.1, 0.2 and 0.05 sec, respectively. To construct three-dimensional images, z-stack images were deconvoluted in softWoRx (GE Healthcare Life Sciences) and processed using Volocity software (PerkinElmer) or ImageJ (http://rsb.info.nih.gov/ij).

To acquire the initial position-image of the beads, 10% sodium azide was added to kill the cells after the observation.

For interference reflection microscopy (IRM), the excitation filter (555/25 nm for TRITC), beam splitter (standard 4 color), and emission filter (525/50 for GFP) were used. IRM visualizes

the cell-substratum adhesion as dark images (Uchida and Yumura, 2004). The area of the cell-substratum adhesion was measured using ImageJ.

To normalize the cell division stages, the mitosis stage index (MSI) was used. The MSI was calculated from the long axis (L) and short axis (l). The short axis represents the width of the furrow. The MSI is calculated by the following formula.

$$MSI = (L-l) / L$$

When the MSI is 0, the cell shape is round; when the MSI is 1, the cell division is complete. Here, the duration time for cytokinesis is defined as the time from cell rounding up to the final separation.

To examine the colocalization between F-actin and traction stress, the plugin Image Calculator of ImageJ was used.

**Measurement of traction stress**

The traction stress in cytokinesis was examined as previously described (Tseng et al., 2012). Cells were allowed to adhere and divide on the surface of silicone gel substratum attached with florescence beads. From the time series of acquired images, a pair of images of fluorescent beads with and without cells (reference image) was initially combined as an image stack. Two images in the stack were subsequently aligned to correct experimental x-y drift using the ImageJ plugin (Template Matching). The displacement field was then calculated by a particle image velocimetry (PIV) program implemented as an ImageJ plugin. The PIV was performed through an iterative scheme (Basic) with 1st pass PIV parameters (the interrogation window (IW) and searching window (SW) sizes were set to 20 and 30 pixels, respectively, whereas the correlation threshold was 0.60). For PIV post processing, we performed the "Normalized median test and replace invalid by median" feature in the PIV plugin. After obtaining the displacement field from the PIV

analysis, the traction stress map and traction vector map were reconstructed via the Fourier transform traction cytometry (FTTC) method with a setting of regularization factor ($RF = 2 \times 10^{-9}$) (Butler et al., 2002; Sabass et al., 2008).

For poly-lysine coating, 1 or 2 mg/ml of poly-L-lysine (Sigma, MW>300,000) were placed on pre-cleaned coverslips for 30 min; they were then vigorously washed with distilled water. Blebbistatin (Sigma) and latrunculin B (Sigma) were dissolved in dimethyl sulfoxide (DMSO) at 20 mM and 2 mM as stock, respectively. Less than 1% DMSO did not affect the cell morphology and traction force.

The parental strain of HS1 is JH10, and those of other mutant cells are AX2. There was no difference in traction stresses among these parental cells.

## Results

### Measurement of traction stress during cytokinesis

*Dictyostelium* cells have at least three distinct modes of cytokinesis: cytokinesis A, B and C (Fig. 1). We investigated the traction stress (force per unit area) generated during each mode of cytokinesis. For the simultaneous observation of traction stress and actin dynamics, cells that expressed GFP-lifeact, a marker of actin filaments, were placed on an elastic silicone substratum attached with red fluorescent beads on its surface (Fig. 2A). The traction stress was calculated from the displacement of the beads. Fig. 2B-K present typical images of a dividing cell. Fig. 2B and C present a DIC image and a 3D fluorescent image of actin in a wild type cell (AX2), respectively, which were obtained via reconstruction from multiple z-slices acquired using a sectioning microscope. Fig. 2D-F represent dorsal, middle and ventral slices, respectively, which indicate that actin filaments localized at the dorsal and ventral furrow cortex (arrows), as well as in the polar pseudopods. Fig. 2G indicates the initial position of the beads (no stress exerted against the substratum), which was captured after the cell was killed by the addition of sodium azide or after two daughter cells migrated away from the field. Fig. 2H presents an averaged image of bead displacement during cytokinesis, which indicates that beads changed their position near and underneath the cell. Fig. 2I and J indicate the calculated traction map and traction vector map, respectively. The magnitude of the traction stress is presented in color code. Each arrow in the traction map indicates both the magnitude and direction of the traction stress (Fig. 2J). Using these techniques, we compared the traction stresses among the three modes of cytokinesis.

**Traction stress in wild type cells (cytokinesis A)**

Fig. 3A presents typical images (DIC, fluorescence image of GFP-lifeact, traction map and vector map) of a wild type cell (AX2) during cell division. Fig. 3C indicates the time course of the mean traction stress, which is calculated by dividing the integrated absolute value of the traction stress with the cell area (n = 16 cells). Here, the mean traction stress was plotted against the mitosis stage index (MSI). The MSI is calculated from the long axis and short axis (Refer to details in the Materials and Methods) to normalize the cell division time. When the MSI is 0, the cell shape is round; when the MSI is 1, the cell division is complete. The mean traction stress began to increase from the MSI 0.5, the stage in which the cell has an elongated morphology prior to furrowing, and reached a maximum peak immediately prior to cell separation (MSI ~0.9), followed by a decline during the final separation. Actin localization and the traction map were partially overlapped. The vector map indicates that most of the traction stress was directed inward from both polar regions (Fig. 2J and Fig. 3A), which suggests that both daughter halves migrate in opposite directions, thereby exerting traction stress against the substratum towards the cell body. For reference, Fig. 3B presents typical images (DIC, fluorescence image of GFP-lifeact, traction map and vector map) of a migrating AX2 cell, and Fig. 3D indicates the distribution of the mean traction stresses of migrating cells. The magnitude of the mean traction stresses in the migrating cells (29.4 ± 6.4 Pa, n = 16) was similar to the highest magnitude of the traction stresses in the dividing cells (28.1 ± 6.9 Pa, n = 18).

**Traction stress in cytokinesis B**

The traction force during cytokinesis B in myosin II null cells (HS1) was examined. The HS1 cells required a longer time (11.2 ± 2.8 min, n = 54) than the wild type cells (4.6 ± 1.2 min, n = 51) to complete their cytokinesis (the time from rounding-up to final separation), which is

consistent with previous results (Neujahr et al., 1997). Fig. 4A presents typical images (DIC, fluorescence image of GFP-lifeact, traction map and vector map) of a dividing HS1 cell performing cytokinesis B. The HS1 cells exhibited a more flattened morphology than the wild type cells (DIC images in Fig. 4A). The traction vector maps indicate that most of the traction stresses were directed inward from both polar regions. Actin was rich in the polar pseudopod regions and mitosis specific dynamic actin structures (MiDASes), which appeared underneath two nuclei in dividing cells (arrows in GFP-lifeact images of Fig. 4A). MiDASes play an important role in cell-substratum adhesion, particularly in cytokinesis B (Itoh and Yumura, 2007). Larger traction stresses were mainly identified at the base of pseudopods; however, there was no significantly large traction stress at the MiDAS regions.

Fig. 4B indicates the time course of the mean traction stress, which is similar to the wild type cells: The traction stress began to increase from approximately MSI 0.5; it reached a maximum peak immediately prior to cell separation (MSI ~0.9) and declined during the final separation. Interestingly, the average traction stress of the HS1 cells at the peak (38.3 ± 7.9 Pa, n = 19) was significantly higher ($p < 0.01$; paired t-test) than the wild type cells (28.1 ± 6.9 Pa, n = 18).

**Traction stress in cytokinesis C**

After HS1 cells that expressed GFP-lifeact were cultured in a suspension condition for two days, they were settled down on the substratum. During this suspension culture, they became multinucleate because of their deficiency in cytokinesis. When they were allowed to attach to the substratum, most cells began to divide in a multipolar fashion even though they were not in a mitotic phase (cytokinesis C). Fig. 5A presents typical images (DIC, fluorescence image of GFP-lifeact, traction map and vector map) of a dividing multinuclear HS1 cell performing cytokinesis C. A larger traction stress was clearly identified along the base of the leading edges of each

dividing fragment. In cytokinesis C, we did not identify MiDAS underneath the nucleus. The traction vector maps indicate that most traction stresses were directed inward from the leading edges. In this figure, the cell ultimately divided into three daughter cells.

Fig. 5B indicates the time courses of the mean traction stress of cells (n = 14 cells) performing cytokinesis C. The cells exhibited fluctuations in the magnitude of the traction stress over time. The mean traction stress was 40.5 ± 11.8 Pa (n = 14), which is similar to HS1 cells performing cytokinesis B.

**Comparison of traction stress and actin structures among three modes of cytokinesis**

Fig. 6A presents a summary of the mean traction stresses in three modes of cytokinesis. The values were derived from the maximum peak values in each dividing cell. Interestingly, the HS1 cells exerted a significantly larger mean traction stress than the wild type cells, and there was no significant difference between cytokinesis B and C.

Fig. 6B presents typical images of actin fluorescence images and a traction vector map in the three different modes of cytokinesis. The vector map indicates that most traction stresses were directed inward. Fig. 6B (Colocal) presents colocalization of actin and the traction stress. In most cases, actin localization and the traction map overlapped along the base of polar pseudopods. However, there was no larger stress in the furrow region in all three modes.

To investigate the role of actin in the traction stress, the traction stresses were assessed when the HS1 cells were treated with latrunculin B, a cell-permeable actin polymerization inhibitor. Within approximately 5 min after the drug application, the subcellular localization of actin was lost, the cells became spherical, and they exerted almost no traction stresses (Fig. 6C), which suggests that the traction stresses depend on the polymerized actin.

To investigate the role of myosin II ATPase activities, the traction stresses were assessed when the wild type cells were treated with blebbistatin, an inhibitor of myosin II ATPase. They became more flat in shape similar to HS1 cells performing cytokinesis B (Fig. 6D). Interestingly, they increased the mean traction stress in the presence of blebbistatin to a level comparable to the HS1 cells. Even under the inhibition of ATPase activities, myosin II has an ability of actin-crosslinking (Laevsky and Knecht, 2003). The experiments using blebbistatin and the results of the HS1 cells indicate that the increase in the traction stress is not a result of the loss of the actin crosslinking activities but is a result of the loss of the motor activities of myosin II.

**Imbalance of traction stress during failed cytokinesis**

The HS1 cells performing cytokinesis B failed to divide on substratum more frequently than the wild type cells: 7.6 ± 0.1% (n = 3, 249 cells) for the HS1 cells and 1.3 ± 0.1% (n = 3, 157 cells) for the AX2 cells on the surface of a plastic dish ($P < 0.01$, paired t-test). Even if the HS1 cells succeeded in cell division, they frequently divided unequally (frequency: 11.6% (n = 3, 249 cells) on the surface of the plastic dish and 14.8% (n = 3, 128 cells) on the silicone gel). The size of each daughter cell was often relatively different; however, each cell had a nucleus in the unequal cell division. In the case of failed cytokinesis B, a daughter half was pulled by another half and fused into one cell; the fused cell eventually migrated to one direction. On the other hand, the wild type cells always divided equally. Fig. 7A presents a typical time course during failed cytokinesis of an HS1 cell (fluorescence image of GFP-lifeact, traction map, and vector map). The force imbalance between the two halves may cause the failure of cytokinesis or unequal cytokinesis.

To clarify this point, the integrated traction stresses were examined in two halves of dividing HS1 cells. Fig. 7B-D indicate the typical time courses of DIC images and the integrated traction stresses of each half during proper (equal) cytokinesis, unequal cytokinesis, and failed cytokinesis.

The traction stresses were almost evenly exerted in both halves in the successfully dividing cell (Fig. 7B). Moreover, in unequal cytokinesis, the small and large halves exerted equal integrated traction stresses (Fig.7C). In contrast, in the failed cases, the integrated stress of the losing half declined, and the remaining half maintained a high level of traction stress (Fig. 7D).

Therefore, the balance of the traction stress between both daughter halves is essential for the success of cytokinesis. Taken together, myosin II must contribute to the equal division of the cytoplasm.

**Wild type cells may exert larger stresses**

As previously described, the wild type cells exerted smaller stresses than the HS1 cells. Why is the power of the wild type cells smaller than the HS1 cells, whereas they have myosin II, a power-generator?

HS1 cells more strongly adhere to the substratum than wild type cells (Jay et al., 1995). Myosin II contributes to the detachment of the cell body from the substratum as one of its functions (Jay et al., 1995). What occurs in the traction stresses when the attachments artificially increase? Bastounis et al. (2014) reported that the lateral stress of migrating cells increases under condition with increased adhesiveness of substratum. To increase the cell-substratum adhesive strength, the substratum was coated with various concentrations of poly-lysine. Fig. 8A presents typical DIC and interference reflection microscopic (IRM) images of dividing AX2 cells on substratum coated with poly-lysine. The IRM images suggest that the attachment area of the cell increased along with the increasing concentration of the poly-lysine coat (0, 1, and 2 mg/ml). In the case of the HS1 cells, the attachment area was substantially larger than that of the AX2 cells on the non-coated surface. Fig. 8B provides a quantitative summary of the attachment area of the AX2 and HS1 cells

with various concentrations of poly-lysine coating. In contrast to the responses of the AX2 cells, the HS1 cells did not increase the attachment area along with the increase of the coating.

On substrata with different coating conditions, the traction stresses were compared between AX2 and HS1 cells (Fig. 8C, AX2 and HS1). Interestingly, the AX2 cells increased the mean traction stress that accompanied the increasing concentration of poly-lysine. They must need to exert larger forces, which are necessary to change the adhesion sites by repeating attaching and detaching. To accomplish this, they also must have mechanosensing to determine the amount of forces required to exert. Interestingly, HS1 cells exhibited a constant magnitude of traction stresses irrespective of the increasing adhesiveness. Thus, myosin II contributes to the increase of the traction force in AX2 cells responding to the substratum adhesiveness. We have previously reported that PTEN (phosphatase and tensin homolog) is an upstream mechanosensing signal for myosin II (Pramanik et al., 2009). PTEN null cells did not increase the mean traction stress when the cell-substratum adhesiveness was increased (Fig. 8C, PTEN-). The assembly and motor activities of myosin II are enhanced by dephosphorylation of its heavy chains (Egelhoff et al., 1993). The expression of 3ALA myosin II (phosphorylatable three threonine residues are exchanged with alanines) in HS1 cells did not rescue the properties of HS1 cells, which suggests that the phosphorylation-regulation of myosin II is crucial for the power-regulation. We also examined two mutant cells deficient in cytokinesis and related to mechanosensing: cortexillin A/B null cells and rac E null cells (Gerald et al., 1998; Weber et al., 1999; Ren et al., 2009). In both cases, they did not increase their traction stresses with the increasing substratum adhesiveness. Among these mutants, the PTEN null cells and rac E null cells frequently divided unequally (6.9% (n = 172) and 26.5% (n = 170), respectively) or failed in cytokinesis (6.9% (n = 172) and 7.1% (n = 170), respectively).

Therefore, wild type cells may regulate the traction force according to their necessity to divide, which likely occurs by sensing the cell-substratum attachment strength and their own force by their mechanosensing. This mechanism may also contribute to the equal division of the cytoplasm during cytokinesis. Myosin II, PTEN, cortexillin A/B, and rac E may contribute to this sensing and regulation.

## Discussion

In the present study, the traction stress and actin localization in the three modes of cytokinesis were investigated via traction force and fluorescence microscopies. To our knowledge, there are limited references regarding the measurements of traction force during cell division. Burton and Taylor (1997) observed the traction force during the cell division of fibroblasts from the wrinkles on the elastic substratum. The traction force increased during the furrowing after rounding up and decreased during the final cleavage, which was similar to the present findings of dividing *Dictyostelium* cells. Tanimoto and Sano (2012) measured the traction stress of dividing *Dictyostelium* cells using poly-acrylamide gel embedded with fluorescent beads, which is a more reliable method than the measurement from wrinkles and thus provides more quantitative and detailed force maps. They identified 2-4 spots of a larger traction stress in both polar regions, which were identified in some cases in the present study (Fig. 2I). Lesman et al. (2014) measured the traction stress of dividing fibroblasts in three-dimensional environments (in fibrin gels) embedded with fluorescent beads, which indicated that the contractile forces regulate the orientation of the cell division axis.

In the present study, we compared the traction force and actin dynamics among the three modes of cytokinesis. In all cases, the traction force was directed inward from both polar regions, which indicates that each daughter half exerts the pulling force from the polar region towards the center of the cell body. This result is consistent with the finding that both daughter halves migrate towards opposite directions. The distribution of actin filaments in both polar regions partially colocalized with the area of the higher traction stress (Fig. 6B). Latrunculin B treatment resulted in a complete loss of traction stress (Fig. 6C), which suggests that actin polymerization plays a major role in traction force generation. Both wild type cells treated with blebbistatin and myosin II null cells

exhibited similar magnitudes and localizations of the traction stresses, which indicates that the power by actin polymerization in the polar pseudopods mainly contributes to the pulling force; however, we could not exclude the possibility that other myosins, such as myosin I, may participate in the pulling force (Dai et al., 1999).

Previous studies of cell division have suggested that the retraction fibers or long fibers at the polar regions that remain after cell rounding up contribute to establishing the polarity of mitotic division and the orientation of cytokinesis by transmitting mechanical forces (Lancaster and Baum, 2011). External forces may control the mitotic spindle orientation and polarity of cell division (Fink et al., 2011). We did not identify retraction fibers after cell rounding up; however, there were frequent extensions, such as pseudopods and filopods, in both polar regions after the elongation stage (>MSI 0.5). The direction of traction vectors became well orientated along the cell division axis after the polar pseudopods began to extend, which suggests that traction forces may contribute to the determination of cell division polarity.

Treatment with blebbistatin, an inhibitor of myosin II ATPase, inhibits the generation of contractile forces by Hela cells and *Xenopus* tissue culture cells (Straight et al., 2003). It substantially reduces the traction forces in migrating keratocytes and dividing fibroblasts (Fournier et al., 2010; Lesman et al., 2014). In contrast, in the present study, both myosin II null cells and blebbistatin-treated wild type cells exerted larger forces than wild type cells. Therefore, the constriction force of the actomyosin based contractile ring does not substantially contribute to the traction forces during cell division. The experiments using blebbistatin and the results of the HS1 cells indicated that the increase in the traction force is not a result of the loss of the actin-crosslinking activities but a result of the loss of the motor activities of myosin II. However, previous researches reported that the actin-crosslinking ability of myosin II is important to generate

traction forces (Lombardi et al., 2007; Meili et al., 2010). They measured the traction stress of the cells deficient in myosin II essential light chain (mlcE null), which has 10% of actin-activated ATPase activities of wild type myosin II (Chen et al.,1995). We need more careful experiments regarding the contribution of traction force by the actin-crosslinking ability of myosin II.

Jay et al. (1995) reported that myosin II null cells migrate substantially slower on a poly-lysine coated substratum than wild type cells. These authors speculated that myosin II contributes to the generation of power to detach the cell from the substratum. During cell division, to move towards opposite directions, both daughter fragments must properly change the adhesion sites by repeating the detachment and attachment. The detachment may be deficient in myosin II null cells. In the case of wild type cells, a part of the traction force will be cancelled by these frequent detachments. Moreover, in myosin null cells, the traction forces will be accumulated as each half advances in the opposite directions, which may cause higher traction forces than wild type cells.

We previously showed that migrating myosin II null cells also exerted higher traction stresses than the wild type cells (Uchida et al., 2003), but some researches showed that the wild type cells exert larger stresses than myosin II null cells (Lombardi et al., 2008; Meili et al., 2010). As shown in the present study, this contradiction may be explained by the difference of adhesiveness of substrata (silicone, polyacrylamide, and gelatin) used in each experiment because the wild type cells can change their forces responding to the substratum adhesiveness.

Most mammalian cells adhere to the extracellular matrix through integrin, an integral membrane protein. *Dictyostelium* cells lack genes that encode integrin and FAK (Sebe-Pedros et al., 2010); however, several proteins, such as SibA, SadA, and Pgh2, have been reported as cell-substratum adhesion proteins with integrin or FAK features (Fey et al., 2002; Gebbie et al., 2004; Cornillon et al., 2008). Several other proteins involved in adhesion, such as talin, Rap1, paxillin,

and vinculin, have also been identified in *Dictyostelium* cells. Nagasaki et al. (2009) and Hibi et al. (2004) showed that paxillin, vinculin, and talin A play important roles in cytokinesis B. We have previously reported that actin foci in the ventral membrane are adhesion sites in *Dictyostelium* cells (Uchida and Yumura, 2004). The number of actin foci in HS1 cells was substantially higher than wild type cells, which supports the greater adhesiveness of HS1 cells. The addition of ATP induced the accumulation of myosin II towards actin foci in the isolated membrane-cytoskeleton complex, which suggests that the force generated by the interaction between actin and myosin II may be transmitted to the substratum via actin foci (Yumura and Kitanishi-Yumura, 1990; Yumura and Kitanishi-Yumura, 1992). However, we did not identify a clear localization of traction stresses at the actin foci or MiDASes. It is likely that the traction forces are balanced within each of these sites, and the calculated traction map did not exhibit a higher level. For the same reason, the furrow regions may lack a large traction stress in the traction map.

When the dividing cell succeeded in the separation, the integrated stress was always the same between the two fragments. Even when the cell divided in an unequal fashion, the integrated stress was the same between the large and small haves, which suggests that these forces are balanced between each other. When the cell failed to separate, the proper balance was lost, and the cell became binucleate. Therefore, the cell maintains the force balance via a tag-of-war between the two halves. To achieve this, the cell should sense its own force and regulate the power. Myosin II null cells more frequently failed in cytokinesis with the imbalance of traction forces; thus, myosin II must contribute to this regulation.

How does the cell sense and maintain the balance? When cells are pressed with an agar block, the amount of myosin II accumulation in the furrow increases (Yumura and Uyeda, 2003;

Pramanik et al., 2009; Srivastava and Robinson, 2015), which suggests that the cell may regulate the amount of myosin II in the furrow region according to the resistant force required against the pressure. When a part of a cell is aspirated with a microcapillary, myosin II accumulates along the edge of the aspirated lobe to retract the lobe into the cell (Effler et al., 2006; Pramanik et al., 2009). When dividing cells are perturbed by the aspiration, wild type cells can restore their symmetric shape after the release of the aspiration and complete their cytokinesis; however, myosin null cells cannot complete this process (Effler et al., 2006). The myosin II molecule appears to have a mechanosensing ability; the myosin motor's lever arm acts as a force amplifier with the external force, and thick filament assembly is also force-sensitive (Ren et al., 2009; Linari et al., 2015). We frequently observed that myosin II transiently accumulated at the tips of retracting polar pseudopods of dividing cells. We speculate that myosin II contributes to keep the size of two halves equal.

We have previously proposed that PTEN is a mechanosensing signal transducer for myosin II localization (Pramanik et al., 2009). Ren et al. (2009) also reported that myosin II and cortexillin I cooperatively interact to form the mechanosensory system. The actin filament is another candidate for a mechanosensor because myosin II exhibits enhanced binding to actin filaments under tension and accumulates in subcellular regions of higher stress (Uyeda et al., 2011). Other proteins, such as rac E, and IQGAP proteins have been reported as molecules related to mechanosensing (Robinson, 2010; Kee et al., 2012). The mechano-channel in the cell membrane may also contribute to mechanosensing (Lombardi et al., 2008). The complete picture of the mechanosensing system for proper cell division must be determined in the future.

## References

Bastounis, E., Meili, R., Álvarez-González, B., Francois, J., del Álamo, J.C., Firtel, R.A., Lasheras, J.C., 2014. Both contractile axial and lateral traction force dynamics drive amoeboid cell motility. J Cell Biol 204, 1045-1061

Burton, K., Taylor, D.L., 1997. Traction forces of cytokinesis measured with optically modified elastic substrata. Nature 385, 450–454.

Butler, J.P., Tolic-Norrelykke, I.M., Fabry, B., Fredberg, J.J., 2002. Traction fields, moments, and strain energy that cells exert on their surroundings. Am J Physiol Cell Physiol 282, C595–605.

Chen, T.L., Kowalczyk, P.A., Ho, G., Chisholm, R.L., 1995. Targeted disruption of the *Dictyostelium* myosin essential light chain gene produces cells defective in cytokinesis and morphogenesis. J Cell Sci 108, 3207-321

Choudhary, A., Lera, R.F., Martowicz, M.L., Oxendine, K., Laffin, J.J., Weaver, B.A., Burkard, M.E., 2013. Interphase cytofission maintains genomic integrity of human cells after failed cytokinesis. Proc Natl Acad Sci U S A 110, 13026–13031.

Cornillon, S., Froquet, R., Cosson, P., 2008. Involvement of Sib proteins in the regulation of cellular adhesion in *Dictyostelium* discoideum. Eukaryot Cell 7, 1600–1605.

Dai, J., Ting-Beall, H.P., Hochmuth, R.M., Sheetz, M.P., Titus, M.A., 1999. Myosin I contributes to the generation of resting cortical tension. Biophys J 77, 1168–1176.

De Lozanne, A., Spudich, J.A., 1987. Disruption of the *Dictyostelium* myosin heavy chain gene by homologous recombination. Science 236, 1086–1091.

Effler, J.C., Kee, Y.S., Berk, J.M., Tran, M.N., Iglesias, P.A., Robinson, D.N., 2006. Mitosis-specific mechanosensing and contractile-protein redistribution control cell shape. Curr Biol 16, 1962–1967.

Egelhoff, T.T., Lee, R.J., Spudich, J.A., 1993. *Dictyostelium* myosin heavy chain phosphorylation sites regulate myosin filament assembly and localization in vivo. Cell 75, 363–371.

Fey, P., Stephens, S., Titus, M.A., Chisholm, R.L., 2002. SadA, a novel adhesion receptor in *Dictyostelium*. J Cell Biol 159, 1109–1119.

Fink, J., Carpi, N., Betz, T., Betard, A., Chebah, M., Azioune, A., Bornens, M., Sykes, C., Fetler, L., Cuvelier, D., Piel, M., 2011. External forces control mitotic spindle positioning. Nat Cell Biol 13, 771–778.

Fournier, M.F., Sauser, R., Ambrosi, D., Meister, J.J., Verkhovsky, A.B., 2010. Force transmission in migrating cells. J Cell Biol 188, 287–297.

Fujiwara, T., Bandi, M., Nitta, M., Ivanova, E.V., Bronson, R.T., Pellman, D., 2005. Cytokinesis failure generating tetraploids promotes tumorigenesis in p53-null cells. Nature 437, 1043–1047.

Funamoto, S., Meili, R., Lee, S., Parry, L., Firtel, R.A., 2002. Spatial and temporal regulation of 3-phosphoinositides by PI 3-kinase and PTEN mediates chemotaxis. Cell 109, 611–623.

Gebbie, L., Benghezal, M., Cornillon, S., Froquet, R., Cherix, N., Malbouyres, M., Lefkir, Y., Grangeasse, C., Fache, S., Dalous, J., Bruckert, F., Letourneur, F., Cosson, P., 2004. Phg2, a kinase involved in adhesion and focal site modeling in *Dictyostelium*. Mol Biol Cell 15, 3915–3925.

Gerald, N., Dai, J., Ting-Beall, H.P., De Lozanne, A., 1998. A role for *Dictyostelium* racE in cortical tension and cleavage furrow progression. J Cell Biol 141, 483–492.

Harris, A.K., Wild, P., Stopak, D., 1980. Silicone rubber substrata: a new wrinkle in the study of cell locomotion. Science 208, 177–179.

Hibi, M., Nagasaki, A., Takahashi, M., Yamagishi, A., Uyeda, T.Q.P., 2004. *Dictyostelium* discoideum talin A is crucial for myosin II-independent and adhesion-dependent cytokinesis. J Muscle Res Cell Motil 25, 127–140.

Iijima, M., Devreotes, P., 2002. Tumor suppressor PTEN mediates sensing of chemoattractant gradients. Cell 109, 599–610.

Itoh, G., Yumura, S., 2007. A novel mitosis-specific dynamic actin structure in *Dictyostelium* cells. J Cell Sci 120, 4302–4309.

Iwadate, Y., Yumura, S., 2008. Actin-based propulsive forces and myosin-II-based contractile forces in migrating *Dictyostelium* cells. J Cell Sci 121, 1314–1324.

Jay, P.Y., Pham, P.A., Wong, S.A., Elson, E.L., 1995. A mechanical function of myosin II in cell motility. J Cell Sci 108, 387–393.

Kanada, M., Nagasaki, A., Uyeda, T.Q.P., 2005. Adhesion-dependent and contractile ring-independent equatorial furrowing during cytokinesis in mammalian cells. Mol Biol Cell 16, 3865–3872.

Kee, Y.S., Ren, Y., Dorfman, D., Iijima, M., Firtel, R., Iglesias, P.A., Robinson, D.N., 2012. A mechanosensory system governs myosin II accumulation in dividing cells. Mol Biol Cell 23, 1510–1523.

Kee, Y.S., Robinson, D.N., 2008. Motor proteins: myosin mechanosensors. Curr Biol 18, R860–2.

Knecht, D.A., Loomis, W.F., 1987. Antisense RNA inactivation of myosin heavy chain gene expression in *Dictyostelium* discoideum. Science 236, 1081–1086.

Laevsky, G., Knecht, D.A., 2003. Cross-linking of actin filaments by myosin II is a major contributor to cortical integrity and cell motility in restrictive environments. J Cell Sci 116, 3761–3770.

Lancaster, O.M., Baum, B., 2011. Might makes right: Using force to align the mitotic spindle. Nat Cell Biol 13, 736–738.

Lee, J., Leonard, M., Oliver, T., Ishihara, A., Jacobson, K., 1994. Traction forces generated by locomoting keratocytes. J Cell Biol 127, 1957–1964.

Lesman, A., Notbohm, J., Tirrell, D.A., Ravichandran, G., 2014. Contractile forces regulate cell division in three-dimensional environments. J Cell Biol 205, 155–162.

Linari, M., Brunello, E., Reconditi, M., Fusi, L., Caremani, M., Narayanan, T., Piazzesi, G., Lombardi, V., Irving, M., 2015. Force generation by skeletal muscle is controlled by mechanosensing in myosin filaments. Nature 528, 276–279.

Lombardi, M.L., Knecht, D.A., Lee, J., 2008. Mechano-chemical signaling maintains the rapid movement of *Dictyostelium* cells. Exp. Cell Res. 318, 1850–1859.

Lombardi, M.L., Knecht, D.A., Lee, J., 2008. Mechano-chemical signaling maintains the rapid movement of *Dictyostelium* cells. Exp. Cell Res. 318, 1850–1859.

Martinac, B., 2004. Mechanosensitive ion channels: molecules of mechanotransduction. J Cell Sci 117, 2449–2460.

Meili, R., Alonso-Latorre, B., del Alamo, J.C., Firtel, R.A., and Lasheras, J.C., 2010. Myosin II is essential for the spatiotemporal organization of traction forces during cell motility. Mol Biol Cell 21, 405-417

Nagasaki, A., de Hostos, E.L., Uyeda, T.Q.P., 2002. Genetic and morphological evidence for two parallel pathways of cell-cycle-coupled cytokinesis in *Dictyostelium*. J Cell Sci 115, 2241–2251.

Nagasaki, A., Kanada, M., Uyeda, T.Q.P., 2009. Cell adhesion molecules regulate contractile ring-independent cytokinesis in *Dictyostelium* discoideum. Cell Res 19, 236–246.

Neujahr, R., Heizer, C., Gerisch, G., 1997. Myosin II-independent processes in mitotic cells of *Dictyostelium* discoideum: redistribution of the nuclei, re-arrangement of the actin system and formation of the cleavage furrow. J Cell Sci 110, 123–137.

Oliver, T., Lee, J., Jacobson, K., 1994. Forces exerted by locomoting cells. Semin Cell Biol 5, 139–147.

Orr, A.W., Helmke, B.P., Blackman, B.R., Schwartz, M.A., 2006. Mechanisms of mechanotransduction. Dev Cell 10, 11–20.

Pramanik, M.K., Iijima, M., Iwadate, Y., Yumura, S., 2009. PTEN is a mechanosensing signal transducer for myosin II localization in *Dictyostelium* cells. Genes Cells 14, 821–834.

Ren, Y., Effler, J.C., Norstrom, M., Luo, T., Firtel, R.A., Iglesias, P.A., Rock, R.S., Robinson, D.N., 2009. Mechanosensing through cooperative interactions between myosin II and the actin crosslinker cortexillin I. Curr Biol 19, 1421–1428.

Robinson, D.N., 2010. 14-3-3, an integrator of cell mechanics and cytokinesis. Small GTPases 1, 165–169.

Sabass, B., Gardel, M.L., Waterman, C.M., Schwarz, U.S., 2008. High resolution traction force microscopy based on experimental and computational advances. Biophys J 94, 207–220.

Sebe-Pedros, A., Roger, A.J., Lang, F.B., King, N., Ruiz-Trillo, I., 2010. Ancient origin of the integrin-mediated adhesion and signaling machinery. Proc Natl Acad Sci U S A 107, 10142–10147.

Spudich, J.A., 1989. In pursuit of myosin function. Cell Regul 1, 1–11.

Srivastava, V., Robinson, D.N., 2015. Mechanical stress and network structure drive protein dynamics during cytokinesis. Curr Biol 25, 663–670.

Straight, A.F., Cheung, A., Limouze, J., Chen, I., Westwood, N.J., Sellers, J.R., Mitchison, T.J., 2003. Dissecting temporal and spatial control of cytokinesis with a myosin II Inhibitor. Science 299, 1743–1747.

Tamada, M., Sheetz, M.P., Sawada, Y., 2004. Activation of a signaling cascade by cytoskeleton stretch. Dev Cell 7, 709–718.

Tanimoto, H., Sano, M., 2012. Dynamics of traction stress field during cell division. Phys Rev Lett 109, 248110.

Tseng, Q., Duchemin-Pelletier, E., Deshiere, A., Balland, M., Guillou, H., Filhol, O., Thery, M., 2012. Spatial organization of the extracellular matrix regulates cell-cell junction positioning. Proc Natl Acad Sci U S A 109, 1506–1511.

Uchida, K.S., Kitanishi-Yumura, T., Yumura, S., 2003. Myosin II contributes to the posterior contraction and the anterior extension during the retraction phase in migrating *Dictyostelium* cells. J Cell Sci 116, 51–60.

Uchida, K.S., Yumura, S., 2004. Dynamics of novel feet of *Dictyostelium* cells during migration. J Cell Sci 117, 1443–1455.

Uyeda, T.Q.P., Iwadate, Y., Umeki, N., Nagasaki, A., Yumura, S., 2011. Stretching actin filaments within cells enhances their affinity for the myosin II motor domain. PLoS One 6, e26200.

Uyeda, T.Q.P., Kitayama, C., Yumura, S., 2000. Myosin II-independent cytokinesis in *Dictyostelium*: its mechanism and implications. Cell Struct Funct 25, 1–10.

Weber, I., Gerisch, G., Heizer, C., Murphy, J., Badelt, K., Stock, A., Schwartz, J.M., Faix, J., 1999. Cytokinesis mediated through the recruitment of cortexillins into the cleavage furrow. EMBO J 18, 586–594.

Yumura, S., Kitanishi-Yumura, T., 1990. Fluorescence-mediated visualization of actin and myosin filaments in the contractile membrane-cytoskeleton complex of *Dictyostelium* discoideum. Cell Struct Funct 15, 355–364.

Yumura, S., Kitanishi-Yumura, T., 1992. Release of myosin II from the membrane-cytoskeleton of *Dictyostelium* discoideum mediated by heavy-chain phosphorylation at the foci within the cortical actin network. J Cell Biol 117, 1231–1239.

Yumura, S., Matsuzaki, R., Kitanishi-Yumura, T., 1995. Introduction of macromolecules into living *Dictyostelium* cells by electroporation. Cell Struct Funct 20, 185–190.

Yumura, S., Mori, H., Fukui, Y., 1984. Localization of actin and myosin for the study of ameboid movement in *Dictyostelium* using improved immunofluorescence. J Cell Biol 99, 894–899.

Yumura, S., Uyeda, T.Q.P., 2003. Myosins and cell dynamics in cellular slime molds. Int Rev Cytol 224, 173–225.

Zang, J.H., Cavet, G., Sabry, J.H., Wagner, P., Moores, S.L., Spudich, J.A., 1997. On the role of myosin-II in cytokinesis: division of *Dictyostelium* cells under adhesive and nonadhesive conditions. Mol Biol Cell 8, 2617–2629.

## Acknowledgements

I would like to express my deepest sense of gratitude to my supervisor Professor Dr. Shigehiko Yumura for his scholastic guidance throughout my research and for writing this thesis paper. I am indebted to Dr. T. Q. P. Uyeda and Dr. T. Kitanishi-Yumura for their valuable discussions. I would also like to thank Dr. Q. Tseng for helping us use the PIV software. I am thankful to dictyBase.org and members of the community for providing several mutants. I am also grateful to Dr. M. Iijima for providing PTEN null cells. I would also like to extend my sincere thanks to Mr. Koushirou Fijimoto, Mst. Shaela Pervin and Mr. Tatsuro Sugiyama and other students of our laboratory for their cordial help and cooperation throughout my research work.

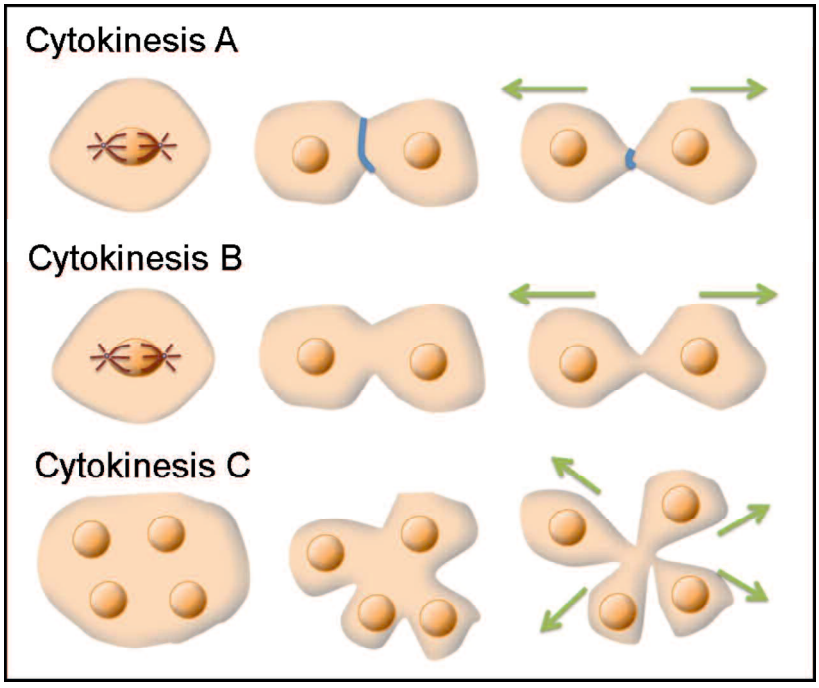


**Fig. 1 Three modes of cytokinesis in *Dictyostelium* cells**

*Dictyostelium* cells have multiple modes of cytokinesis: cytokinesis A, B and C. In cytokinesis A, a conventional 'purse string model', the constriction of the contractile ring (thick blue lines) composed of actin and myosin II in the cleavage furrow splits a cell into two daughter cells. Cytokinesis B and C are dependent on the traction force against the substratum. Cytokinesis A and B are dependent on the cell-cycle in contrast to cytokinesis C.

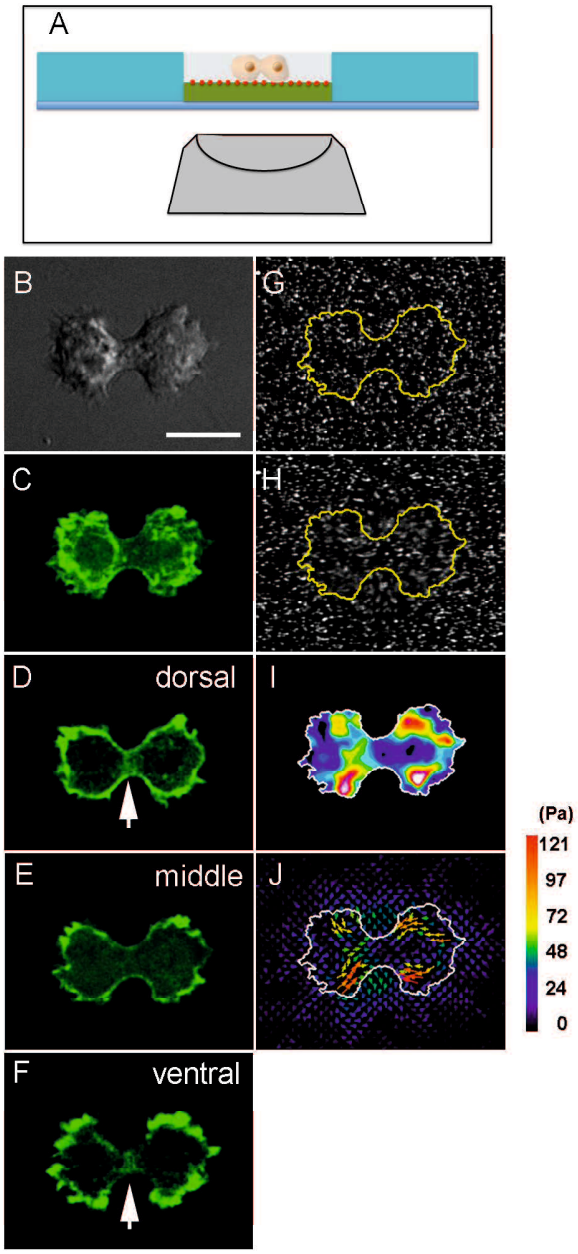


**Fig. 2 Traction force microscopy**

(A) For traction force microscopy, *Dictyostelium* cells (AX2) that expressed GFP-lifeact, a marker of actin filaments, were placed on elastic silicone substratum (green) attached with red fluorescent beads to its surface. The cell and bead movements were observed under a sectioning microscope. (B) DIC and (C) 3D reconstituted fluorescence images from 9 z-slices of a dividing cell. Panels (D), (E), and (F) present dorsal, middle and ventral slices, respectively, which indicate that actin filaments localized at the dorsal and ventral furrow cortex (arrows), as well as the polar pseudopods. Panels (G) and (H) show fluorescence images of beads. Panel G represents the initial positions of the beads (no stress exerted against the substratum), which was captured after the cells were killed by the addition of sodium azide. Panel H represents an averaged image of the bead displacement during cytokinesis, which indicates that beads changed their position near and underneath the cell. The cell boundary is indicated by yellow lines. Panels (I) and (J) present the calculated traction map and traction vector map, respectively. The color code indicates the intensity of the traction stress. Bar, 10 μm.

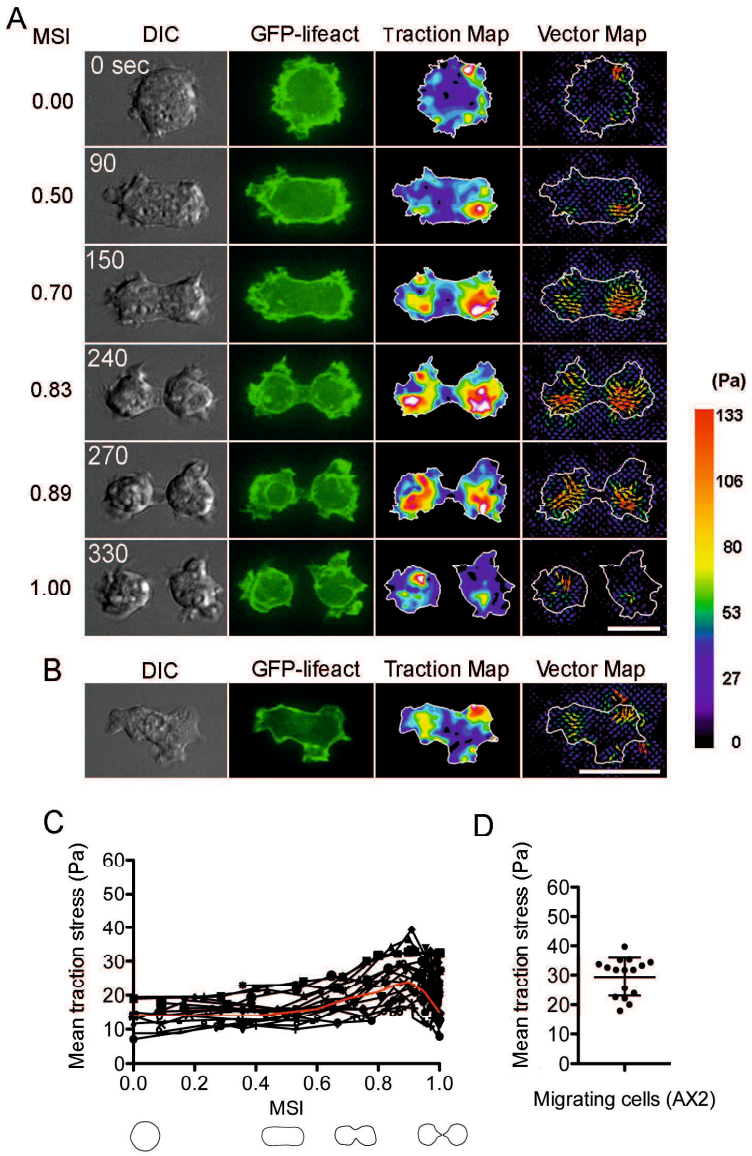


**Fig. 3 Traction stress in wild type cells**

(A) Typical images (DIC, fluorescence image of GFP-lifeact, traction map and vector map) of a wild type cell (AX2) during cell division (from rounding to final separation). (B) Typical images (DIC, fluorescence image of GFP-lifeact, traction map and vector map) of a migrating wild type cell. (C) Time course of the mean traction stress of multiple dividing cells (n =18). Mitosis stage index (MSI) is used to normalize the cell division time. Note that the traction stress began to increase from MSI 0.5, the stage in which the cell morphology is elongated prior to furrowing; it reached a maximum peak immediately prior to cell separation (MSI ~0.9) and declined during the final separation. The red line indicates the time course of the averaged mean traction stress of 18 cells. (D) A summary of the mean traction stresses in migrating cells (n = 16). Bars, 10 μm.

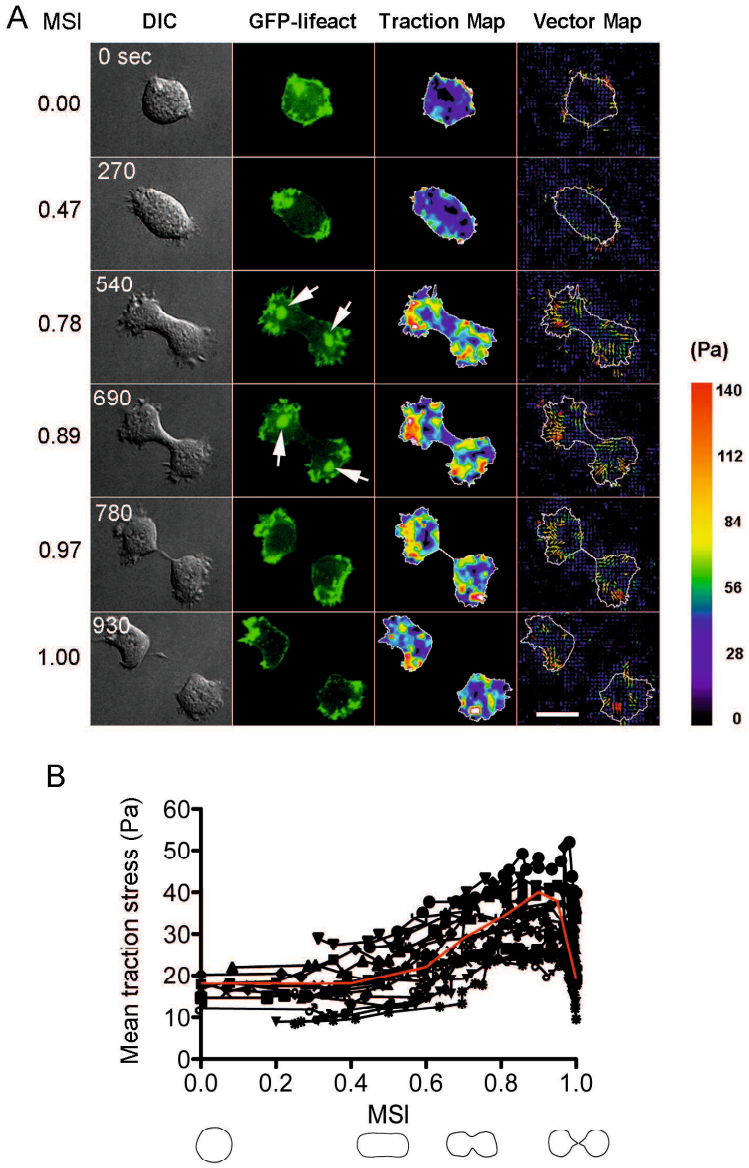


**Fig. 4 Traction stress in cytokinesis B**

(A) Typical images (DIC, fluorescence image of GFP-lifeact, traction map and vector map) of a dividing myosin null cell (HS1, cytokinesis B). White arrows indicate mitosis specific dynamic actin structures (MiDASes), which mainly appeared in cytokinesis B. (B) Time course of the mean traction stress of multiple cells (n =19). The traction stress began to increase from approximately MSI 0.5; it reached a maximum peak immediately prior to cell separation (MSI ~0.9) and declined during the final separation. The red line indicates the time course of the averaged mean traction stress of 19 cells. Note that the averaged traction stress of the HS1 cells at the peak was significantly higher than the wild type cells. Bar, 10 μm.

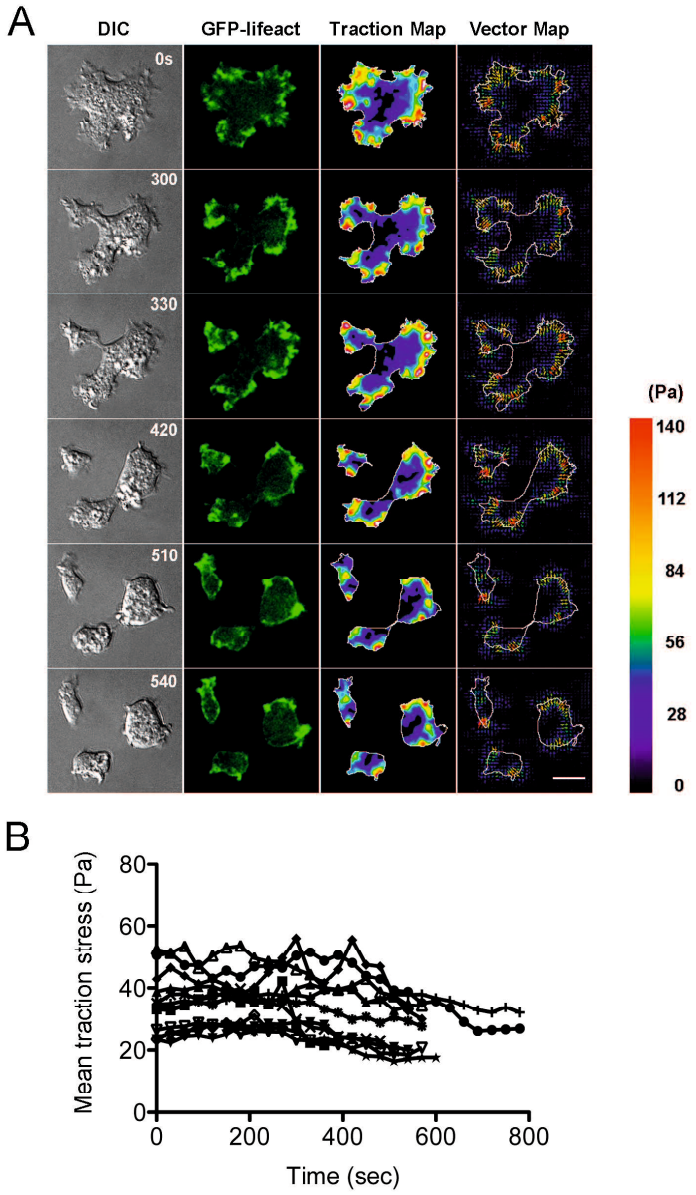


**Fig. 5 Traction stress in cytokinesis C**

(A) Typical images (DIC, fluorescence image of GFP-lifeact, traction map and vector map) of a dividing myosin null cell (HS1, cytokinesis C). When HS1 cells were allowed to attach to the substratum after shaking-culture for two days, most cells began to divide in a multipolar fashion. Greater traction was clearly identified along the base of the leading edges of each dividing fragment. (B) Time course of the mean traction stress of multiple cells (n =14). In these experiments, time (sec) was used instead of the MSI. The cells exhibited fluctuations in the traction stress magnitude. The averaged traction stress was 40.51 ± 11.89 Pa (n = 14). Bar, 10 μm.

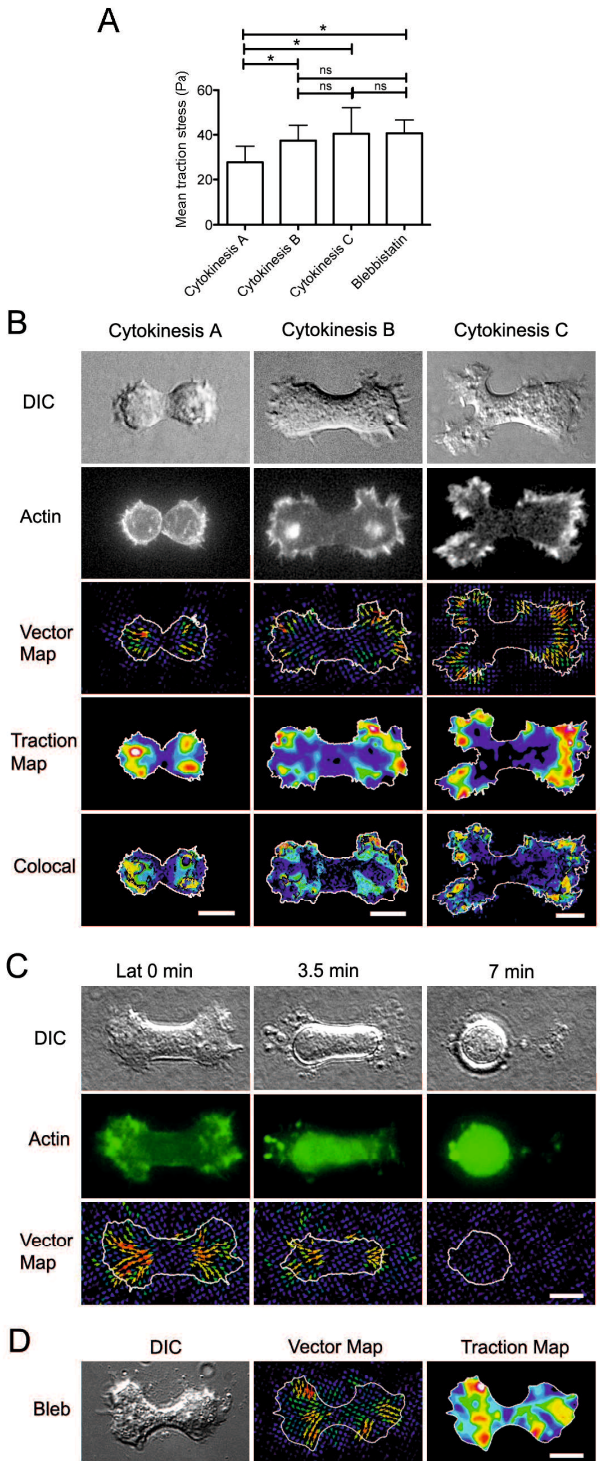


**Fig. 6 Correlation between traction stress and actin structures**

(A) A summary of the mean traction stress in three different modes and the mean traction stress of wild type cells in the presence of 150 μM blebbistatin. (* $P<0.05$, ns: not significant; via 1-way ANOVA Tukey's multiple comparison test, n = 18 for cytokinesis A, n = 19 for cytokinesis B; n = 14 for cytokinesis C; n = 9 for blebbistatin). (B) Comparison of typical dividing cells in three different modes (DIC, fluorescence image of GFP-lifeact, vector map and traction map). Colocalization between actin and traction map is presented (Colocal). In most cases, actin localization and the traction map partially overlapped. Moreover, larger traction stresses were identified along the base of the polar pseudopods. (C) Effect of actin disruption on the traction force. Typical images (fluorescence image of GFP-lifeact and vector map) of an HS1 cell that expressed GFP-lifeact following the application of 10 μM latrunculin B (0, 3.5, and 7 min). Note that the cell became spherical and most traction stresses disappeared 7 min after the application. (D) Effect of blebbistatin on the traction force. The cells were observed from 1 hr after the application of 150 μM blebbistatin because the drug did not exhibit noticeable effects immediately after application. Typical images (DIC, vector map, and traction map) of a wild type cell in the presence of blebbistatin. Note that wild type cells became more flat in shape similar to HS1 cells performing cytokinesis B and increased the mean traction stress in the presence of blebbistatin. Bars, 10 μm.

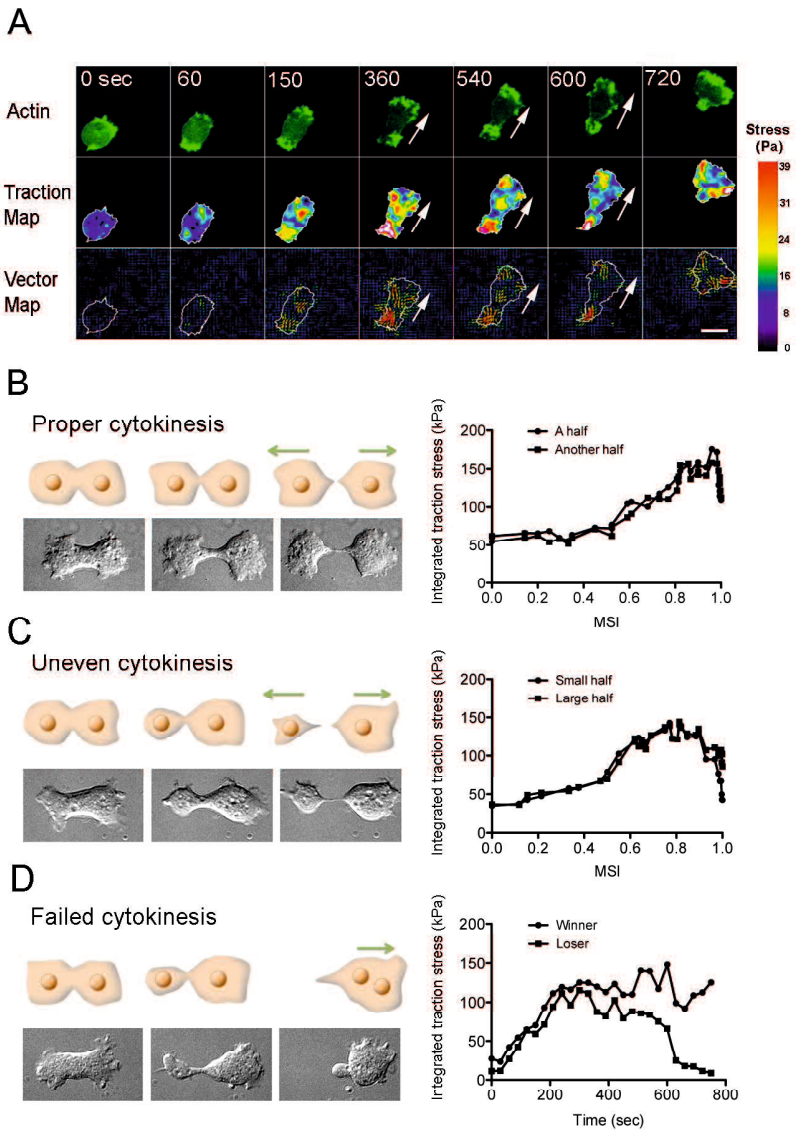


**Fig. 7 Imbalance of traction stress during failed cytokinesis**

(A) Typical images (fluorescence image of GFP-lifeact, traction map and vector map) of a myosin null cell during failure in cytokinesis B. One daughter half was pulled by another half, fused into one cell, and eventually migrated in one direction (arrows). (B) Time courses of DIC and the integrated traction stress in two daughter halves in proper cytokinesis. The traction stresses were almost equally exerted in both halves. (C) Time courses of DIC and the integrated traction stress in two daughter halves in unequal cytokinesis. The small and large halves exerted equal integrated traction stresses. (D) Time courses of DIC and the integrated traction stress in two daughter halves in failure cytokinesis. The losing half declined in the integrated stress, whereas the remaining half maintained a high level of traction stress. Bar, 10 μm.

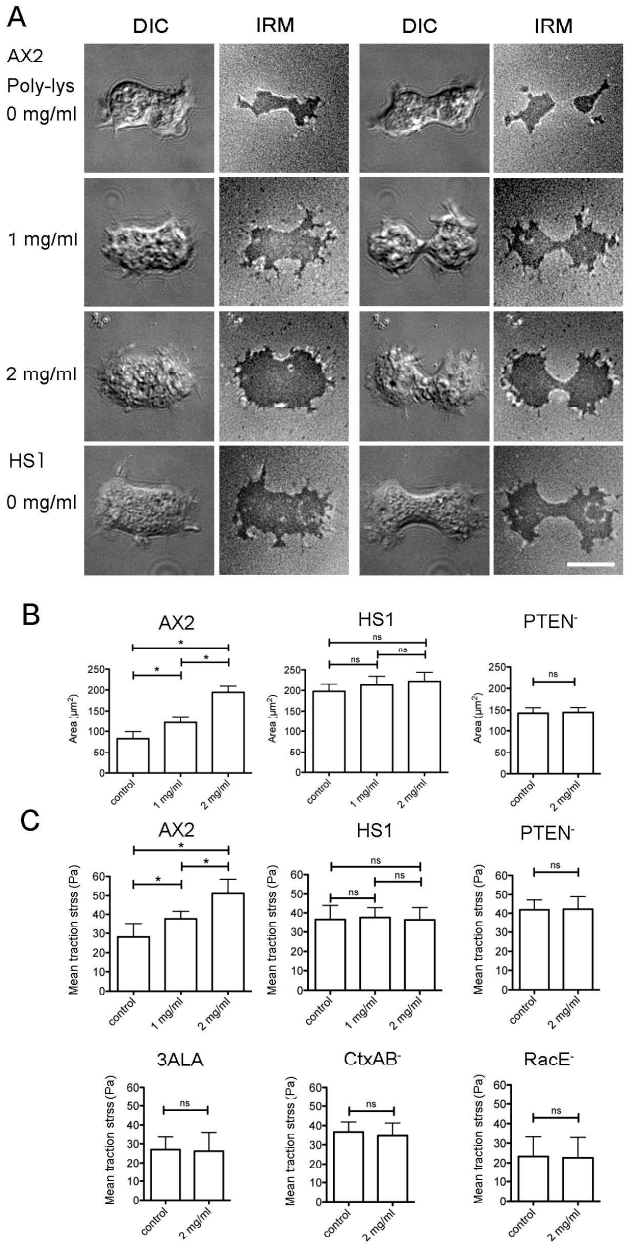


**Fig. 8 Wild type cells may exert a larger stress on higher adhesive substratum**

(A) Typical DIC and interference reflection microscopic (IRM) images of dividing AX2 and HS1 cells on substrata coated with different concentrations (0, 1, or 2 mg/ml) of poly-lysine. Two different mitotic stages are shown for each condition (left and right). (B) Quantitative analysis of the attachment area in AX2, HS1, and PTEN null cells. The attachment area was quantitated from the dark area of the IRM. Note that the attachment area of the AX2 cell increased in accordance with an increasing concentration of poly-lysine coating, whereas the HS1 and PTEN null cells did not increase. (* $P<0.01$, ns: not significant; by 1-way ANOVA Tukey's multiple comparison test, n = 18 per condition for AX2 cells, n = 19 per condition for HS1 cells). (C) Mean traction stresses of AX2 cells, HS1 cells, PTEN null cells, HS1 cells that expressed 3ALA myosin II, cortexillin A/B null cells, and rac E null cells on the substrata coated with different concentrations of poly-lysine. Note that AX2 cells increased the traction stress according to the increasing concentration of poly-lysine in contrast to the other mutant cells. (* $P<0.01$, ns: not significant; by 1-way ANOVA Tukey's multiple comparison test, n = 12 per condition for AX2 cells, n = 19 per condition for HS1 cells; n = 13 per condition for PTEN null cells; n = 17 per condition for HS1 that expressed 3ALA myosin II; n = 11 per condition for cortexillin A/B null cells; n = 11 per condition for rac E null cells). Bar, 10 μm.